International Journal of
INTELLIGENT SYSTEMS AND APPLICATIONS IN ENGINEERING
ISSN:2147-6799 www.ijisae.org Original Research Paper

Alzheimer's Disease Classification System of Brain Magnetic Resonance Images based on light weight U-Net Network

K. Ranga Swamy*[1], S. Senthilkumar[2]

Submitted: 28/01/2024 **Revised**: 02/03/2024 **Accepted**: 12/03/2024

Abstract: Alzheimer's Disease (AD) is a neurodegenerative disease that commonly occurs in older people. Recently, researchers created a novel approach based on deep learning, a branch of machine learning, for the instinctive analysis of AD. It is characterized by both cognitive and functional impairment. However, as AD has an unclear pathological cause, it can be hard to diagnose with confidence. This is even more so in the early stage of Mild Cognitive Impairment (MCI). Accurate and rapid classification of AD is critical for the diagnosis and treatment of elder patients. However, MRI images often present challenges such as variable size and shape, low contrast, blurred boundaries, and numerous shadows. To address these issues, In this research article, we propose a lightweight U-Net architecture(LW-Unet) for the classification of AD. We add residual blocks, and residual convolutional layer pathways are integrated into the atrous spatial pyramid pooling (ASPP) module and Multi-Scale Context Fusion Block (MSCFB). To fuse convolutional feature maps in encoding layers, the ASPP unit used a learnable set of parameters. An efficient architecture for feature extraction during the encoding step is the ASPP unit. We integrated the AD unit with the benefits of the U-Net network for deep and shallow features. A mixed loss function composed of Dice loss, Bce loss, and Focal loss functions is used. The experimental results are validated using the Sensitivity, PPV, Dice similarity coefficient(DSC), and IOU values. The AD classification accuracy of the proposed method LW-Unet is 98.40, and 98.91 in the ADNI and NACC Data sets respectively. The results show a good performance of the proposed MLCNN model in terms of dice similarity coefficient criteria and IOU value..

Keywords: dementia; deep neural network (DNN); medical image processing; Alzheimer's disease (AD); brain imaging

1. Introduction

Dementia is a general term for a loss of memory, language, problem-solving and other thinking skills that are severe enough to affect daily life. The commonest causes of dementia include Alzheimer's disease (AD), vascular dementia (VaD), and dementia with Lewy bodies (DLB)[1-2]. Both the prevalence and incidence of dementia increase with advancing age, but about 5% of cases have onset at age all currently available treatments may only delay its progress. Nonetheless, the diagnosis of AD, especially in the early stages, is important, so that individuals and families can be aware and make adjustments to their lives as needed, but also since more precise diagnosis will be needed to develop new, potentially disease-modifying treatments[3].

In general, mild cognitive impairment (MCI) represents the early stage of AD. Patients diagnosed with MCI are more likely to progress to AD with a ratio of about 16% developing AD within about 4 years, compared with non-MCI subjects whose conversion rate is about 1-2% in this period[4]. However, not all people diagnosed with MCI will progress to AD and some will remain stable or even return to normal cognition, which indicates that MCI can be further divided into two categories: progressive MCI (pMCI) and stable MCI (sMCI), according to the future risk of progressing to AD in future years. Therefore, identifying MCI and its sub-categories (pMCI and sMCI) should have a significant impact on the early stage of treatment to mitigate the progress of dementia. AD, as a neurodegenerative disease whose pathologic cause is unclear, is hard to identify with certainty by noninvasive clinical investigations[5-6].

Clinical diagnosis usually relies on a combination of history, mental state examination, and cognitive testing. The most commonly used cognitive instrument for AD diagnosis has been the Mini-Mental State Examination (MMSE), which is a short questionnaire testing a range of cognitive domains. However, despite having quite high sensitivity and specificity for dementia, the MMSE performs less well with early-stage MCI [7]. The most commonly used cognitive instruments for the diagnosis of AD and MCI are Mini-Mental State Examination (MMSE), and MoCA[8-9]. These cognitive assessment tools are short questionnaires to test a range of cognitive domains. However, despite having relatively high sensitivity and specificity for dementia, they perform less well in the diagnosis of early-stage MCI[10]. Further, their scores are affected by educational level and language, and therefore, they are insufficiently objective as a means of diagnosis. The sampled brain MR image is given in Figure 1.

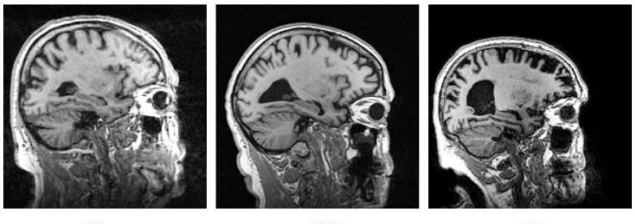

Figure 1. Sample brain MR image of a CN, MCI, and AD patient.

[1] *Research scholar, Department of CSE, Presidency University, Bangalore Email: rangaswamyphdcse@gmail.com*
[2] *Professor, Department of CSE, Presidency University, Bangalore Email: harisen1234@yahoo.co.in*
** Corresponding Author Email: rangaswamyphdcse@gmail.com*

Recently, machine learning technology has shown promising performance in AD incidence prediction with large-scale administrative health data (Park et al., 2020). A more objective approach to AD diagnosis is through biomarkers such as brain imaging [11-13], and blood and cerebrospinal fluid examination. However, due to the unclear pathological cause, there is no uniform standard for AD diagnosis through biomarkers. Applying such tests for MCI is even less precise because of the heterogeneity of the syndrome of MCI. Consequently, with the development of artificial intelligence in the field of computer vision, computer-aided AD diagnosis, including prediction of AD and MCI, using medical images has become a research hotspot in recent years[14-15]. Some recent studies have shown its capability in AD diagnosis with various modalities of radiography as input including structural MRI (sMRI), functional MRI (fMRI), and positron emission tomography (PET). The remaining portions of the paper were assembled as follows: Section 2 gives a review regarding feature extraction as well as the categorization of AD diagnosis. Section 3 explains the proposed LW-Unet methodology. Section 4, elaborates on the experimental results, comparisons, and discussions, followed by Section 5, which concludes the paper.

2. RELATED WORK

Detailed preprocessing with refined extraction of biomarkers combined with statistical analysis is the accepted practice in current medical research. In their study of biomarkers derived from T1-weighted MRI scans of AD, MCI, and HC using voxel-based morphometry and parcellation methods, Risacher et al. The study indicates statistical significance in a number of measurements, including entorhinal cortex thickness and hippocampal volume. This significance was further supported by Qiu et al(2009)[16] who used large deformation diffeomorphic metric mapping (LDDMM) to examine regional volumetric changes. In order to find microRNA biomarkers in various stages of Alzheimer's disease, Guevremont et al(2022)[17] concentrated on robustly detecting microRNAs in plasma and employed standardized analysis. This study's statistical analysis produced valuable diagnostic markers that represent the pathology of the underlying disease. To detect changes in biomarkers during disease progression, various biomarker information was retrieved and fed into statistical analysis methods with changing numbers of variables. Other neuroimaging data, genetic information, and CSF biomarkers were used in similar investigations. This research established the rationale for MRI imaging biomarkers in the diagnosis of AD and MCI and provided the groundwork for the creation of automatic diagnostic algorithms.

Due to its ability to adapt to data and generalize information with less need for expert experience, machine learning has become one of the most prominent automated diagnostic methods in use today. Through a performance comparison between the Support Vector Machine (SVM) categorization of local grey matter volumes and human diagnosis by qualified radiologists, the work by Klöppel et al (2018)[18] demonstrated the usefulness of using machine learning algorithms in detecting dementia. Using penalized regression with resampling, Janousova et al(2013)[19] suggested looking for discriminative regions to help Gaussian kernel SVM classification. The study's regions were those previously identified by morphological investigations. These innovations sparked the creation of numerous machine-learning algorithms for the identification of AD and MCI[20-21].

A kernel combination technique was put out by Zhang et al (2011)[20] for the fusing of diverse biomarkers for classification using a linear SVM. The Multifold Bayesian Kernelization (MBK) approach was proposed by Liu et al. [25] and uses a Bayesian framework to compute kernel weights and synthesis analysis to yield diagnostic probability for each biomarker. Particle swarm optimization (PSO), Welch's t-test (WTT), a polynomial kernel SVM, and Zhang et al.'s [26] proposal for extracting the eigenbrain were used. With the help of CNN deep learning algorithms, Gorji and Naima (2019)[21] were able to distinguish between EMCI and LMCI with 93% accuracy, 91.48% sensitivity, and 94.82% specificity using sagittal characteristics from an MRI picture. Additionally, Nozadi and Kadoury (2018)[22] used the ADNI dataset to examine the FDG and AV-45 biomarkers of the PET picture and then used RBF-SVM and RF to separate AD, NC, EMCI, and LMCI into six groups. Their method demonstrated accuracy for AD versus NC using RBF-SVM and RF with FDG-PET imaging modalities of 91.7% and 91.2%, respectively.

The OASIS dataset was utilized for comparison, while Gupta et al (2019) [23] offered a solution using the GARD dataset as a known private dataset. According to the classifier, the four classifiers produced better results when used for binary and tertiary classification. The softmax classifier demonstrated the greatest accuracy of 99.34%, 100% specificity, and 100% precision for AD against HC. The SVM classifier had a 99.2% accuracy, 100% specificity, and 100% precision for the HC versus mAD instance. Good results were also obtained using the mAD against aAD SVM, including 97.77% accuracy, 100% sensitivity, and 97.95% F1 score. SVM had the highest accuracy of 99.42%, 99.18% sensitivity, and 99.99% precision in AD against HC versus mAD for tertiary classification.

3. PROPOSED METHODOLOGY

In this section, we provide a brief introduction to the main processing frameworks of this paper as follows: the full convolution structure for the generator and the discriminator structure are provided, and in addition, a combined loss function based on reducing category imbalance is then introduced.

3.1 Data preprocessing

The classification accuracy will be inadequate due to the morphological diversity of brains, such as high variability of brain location, boundary ambiguity, and deviation from manual annotations, therefore preparation of brain data is very important. 3D Brain image size is 240×240×155. In our data preprocessing step, invalid pixels of brain images are first removed, and then each 3D image data is sliced into a number of 2D images. Then, every patch with a size of 128×128 is extracted on each 2D slice. Simultaneously, Z-score regularization to regularize irregular brain s is used to lessen the intensity difference between distinct brain slices, which is described in Eqn(1):

$$z' = \frac{z - \mu}{\delta} \tag{1}$$

where z is the input image, z' is the normalized image, μ is the average value of the input image, and δ is the standard deviation of the input image.

3.2 AD classification using Lightweight U-Net

In terms of classification performance, an improved U-Net network for AD MRI image classification, that is, the Lightweight Unet (LW-Unet) network, is constructed, and the U-Net network

is improved at the structural and non-structural levels. The goal of high accuracy and high precision classification of MRI images of ADs has been realized. In terms of classification efficiency, the LW-Unet network consumes a large amount of storage and computing resources due to the increase in the number of parameters and calculations. It also has the risk of over-fitting, which hinders the classification network from moving toward large-scale clinical applications. In order to solve these problems, the LW-Unet network is lightweight and designed to achieve a good balance between performance and efficiency. The LW-Unet structure is given in Figure 2. Figure 2 shows the network structure of the deep convolutional network Light weight Unet for AD MRI image classification. The main structure of the network is still the encoder and decoder structure of U-Net. The left path of the figure represents down-sampling, and the right path of the figure represents upsampling. There are 4 feature fusion channels between the paths on both sides, and the input is 512 × 512 AD MRI images[24].

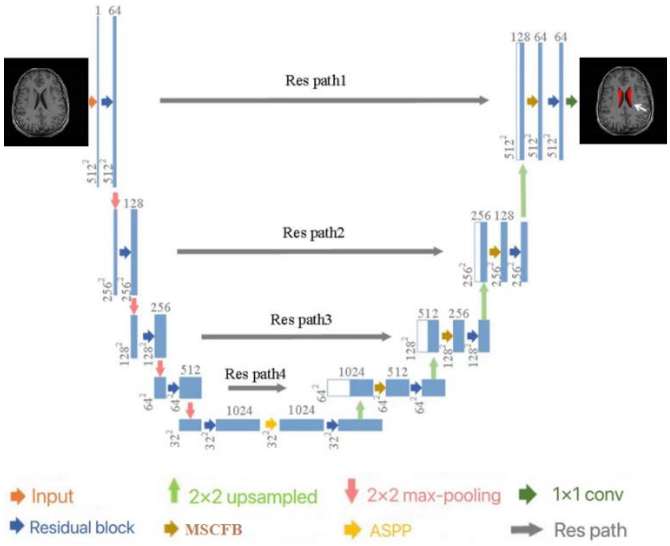

Figure 2. Lightweight Unet network structure

The contraction path consists of 4 groups of residual modules and 4 times 2 × 2 maximum pooling. The use of residual modules can effectively avoid gradient disappearance, accelerate the convergence of the network, and make the network more stable. In the encoding process, every time the residual module is passed, the number of channels of the feature layer is doubled, and the spatial size remains unchanged. Every time a 2 × 2 maximum pooling layer is passed, the spatial size of the feature layer is halved, and the number of channels remains constant. Two residual modules and one ASPP module are connected at the end of the encoding network, which expands the receptive field of the network and avoids the problem of losing edge information due to continuous pooling. The Res Path is introduced in the feature fusion channel so that the feature layer of the encoding network can be cascaded with the feature layer of the decoding network after passing the Res Path. This can reduce the semantic interval between the two parts of the feature layer, and combine the shallow features in the network with deep features. The expansion path includes 4 sets of CBAM attention modules, 4 sets of residual modules and 4 times 2 × 2 upsampling operations. Adding CBAM attention modules can suppress unimportant information in the image and emphasize important features in the image. In the decoding process, when upsampling is performed, the feature layer size is doubled and the number of channels remains unchanged. After the residual module and the CBAM attention module, the feature layer space size remains unchanged while the number of channels is halved. The last layer of the decoding network uses 1 × 1 convolution to reduce the number of feature maps and outputs the classification result map of AD s.

3.2.1 Residual module

In U-Net, as the number of network layers deepens, the network performance improves, but it may face the problem of gradient disappearance, resulting in network degradation. Introducing a residual network can effectively solve this problem [27]. X is the input of the network and $F(X)$ output of the feature extraction module, which $H(X)$ represents the actual mapping. The residual module's output is:

$$H(X) = F(X) + X \tag{2}$$

The residual module consists of a residual learning part and an identity mapping part. The overall operation process is: convolution, batch normalization (BN) operation, leaky rectified activation function (Leaky ReLU), convolution, BN operation, Leaky ReLU, this module can not only speed up convergence speed, and effectively solve the problem of network model degradation.

3.2.2 Res path

The original U-Net network can take into account richer global information prediction and more local detail prediction. However, in the AD MRI image classification task, it is necessary to fuse the underlying semantic features with the high-level semantic features, skip the connection will cause the incompatibility of the two features. There will be semantic differences, which will adversely affect the classification effect of the image. In response to this problem, the introduction of Res Path into the U-Net network can apply the residual idea to the feature propagation path, cascade the feature layers on the encoding and decoding path, and fuse two different semantic features.

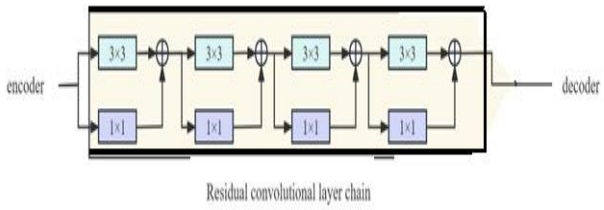

Figure 3. Res Path structure

The overall structure of the residual convolutional layer chain is shown in Figure 3. Res Path consists of four 3 × 3 convolutional layers and a 1 × 1 residual structure. After the Res Path, the feature layer space size and a number of channels remain the same. As we move towards deep skip connections, the semantic gap between feature maps on the downsampling and upsampling paths shrinks. Thus, the number of convolutional blocks used in the Res Path of the LW-Unet decreases progressively, using 4, 3, 2, and 1 convolutional blocks in Res Path 1, 2, 3, and 4 respectively. The addition of Res Path, a non-linear operation, effectively reduces the semantic difference between the encoder and the decoder,

enabling a better fusion of shallow features and deep features, thereby improving the performance of the model.

3.2.3 ASPP module

In the U-Net network, the feature resolution is negatively correlated with the number of network layers, that is, the feature resolution will decrease as the number of network layers increases. Although the model can learn more advanced semantic information, it is often accompanied by a certain amount of information loss, which is generally not conducive to the progress of the division task. In order to capture more abstract feature information and retain more spatial information, and improve the accuracy of classification, an ASPP module is added to the deepest layer of the U-Net network.

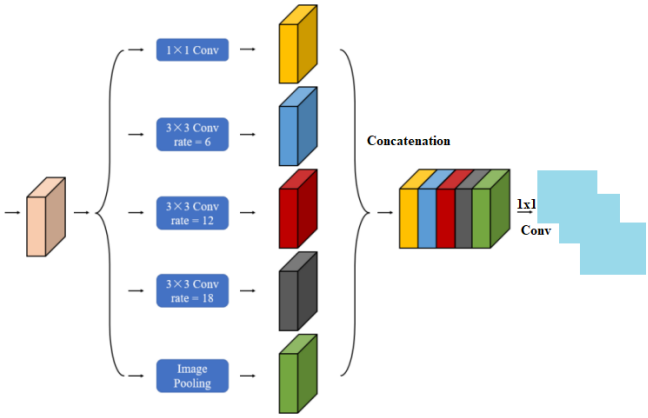

Figure 4. ASPP structure

The workflow of the ASPP module is shown in Figure 4. After the feature map is input, it will enter six parallel branches. The first branch directly performs the convolution operation on the input feature map 1 × 1 to obtain a multi-scale feature map. In the next four branches, the 3 × 3 void convolution expansion rates are 2, 4, 8, and 16 respectively. The last branch is 1 × 1 the linear activation of the convolution. After that, the corresponding pixel addition operation is performed on the obtained six feature maps to obtain the output features picture. The features extracted through different scales of receptive fields are different, which can compensate for the information loss caused by deep convolution and obtain richer abstract information at the same time.

3.2.4 Multi-Scale Context Fusion Block (MSCFB)

The U-Net network in the AD classification task is not ideal, which is largely due to the problems of more shadows and blurred boundaries in AD MRI images. As a lightweight network module, the **MSCFB** module can be easily implanted into other network structures. The MSCFB module can selectively focus on important information in the image, ignore unimportant areas, and apply to Excellent performance in classification tasks. Introducing the MSCFB attention mechanism into the decoding path of the U-Net network can enable the U-Net network to focus on the features of the AD region when performing the classification task of AD MRI images. The specific performance is as follows: During the network training process, the MSCFB module will give a larger weight to the AD region of the image in the convolutional layer through continuous learning so that the network can obtain more AD feature information and achieve the purpose of improving the model classification performance[31].

Continuous convolution and pooling operations can detect feature maps with different scales. Due to the fixed network layers, it has some shortages on multi-scale context extraction. Faced with this issue, a MCF block is proposed for context enhancement to obtain multi-scale spatial context information. Combined with the atrous convolution, it offers a practical way to acquire various receptive fields. Additionally, it produces fewer model parameters than traditional convolution, such as 5*5 convolution, 7*7 convolution, etc. Inspired by this advantage, atrous spatial pyramid pooling (ASPP) block has been proposed to detect multi-scale contexts. However, it exists the grid effect that some image pixels are in the visual blind area, and could not be involved in the information loss to cause the information loss(see Fig.5). Inspired by As the PP block, by stacking four 3*3 atrous convolutions, the MCF block is proposed for MA classification. For the MCF block, combined with atrous convolution, four parallel network branches are built for multi-scale feature representation, and the dilation rates for four atrous convolution layers are set as 1, 3, 5, and 7. The specific mathematical description is given in Eq.(3).

$$
\begin{aligned}
H_{c1} &= F_{d1}(H_a) \\
H_{c2} &= F_{d3}(H_{c1} \Theta H_a) \\
H_{c5} &= F_{d5}(H_{c2} \Theta H_{c1} \Theta H_a) \\
H_{c4} &= F_{d7}(H_{c5} \Theta H_{c2} \Theta H_{c1} \Theta H_a)
\end{aligned} \tag{3}
$$

where Fd1 represents the 3*3 atrous convolution of the dilation rate of 1, Fd3 represents the 3*3 atrous convolution of the dilation rate of 3, Fd5 represents the 3*3 atrous convolution of the dilation rate of 5, Fd7 represents the 3*3 atrous convolution of the dilation rate of 7. Ha represents the input feature maps, and (Hc1, Hc2, Hc3, Hc4) represents the four output feature maps from four parallel network branches. Meanwhile, the global pooling layer is also introduced to acquire the average of the global contexts. The final output of the proposed MCF block is defined as per Eqn (4).

$$
H_m = G(H_a) \Theta H_{c4} \Theta H_{c3} \Theta H_{c2} \Theta H_{c1} \tag{4}
$$

where G represents the network branch with global pooling.

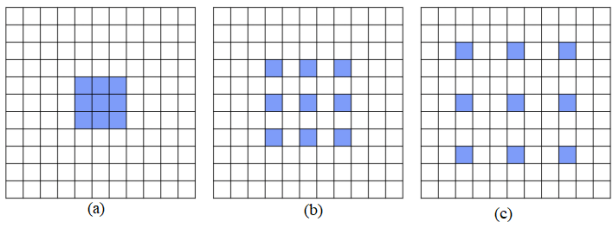

Fig. 5: Grid effect on cascaded atrous convolution. (a) 3*3 atrous convolution; (b) Two cascaded 3*3 atrous convolution; (c) Three cascaded 3*3 atrous convolution.

3.2.5 Loss function

The loss function is used to evaluate the difference between the predicted value of the model and the real value. The loss function gradually converges, which means that the training of the model has reached a better level. Therefore, it is also very important to choose an appropriate loss function. In this paper, the absolute error loss $L1$ and the minimization of the perceptual loss Lp are thoroughly examined, and a loss function appropriate for

Colonoscopy images is developed. As we all know, norm loss functions $L1$ and $L2$ will have fuzzy problems regarding image classification. The loss function L_1 , the minimum absolute deviation function, has higher robustness and less fuzziness than the loss function L_2. Therefore, we introduce L_1 to encourage the network to segment an image with higher similarity to the ground truth image by measuring the pixel-level value difference between them. The loss function is as follows:

$$L_1 = \mathcal{L}(\hat{I}, I^*) = \sqrt{\left\|\hat{I} - I^*\right\|^2 + \varepsilon^2} \tag{5}$$

where $\hat{I}$ and $I*$ represent segmented images and ground truth images from the training dataset, respectively; ε represents the error offset. The perceptual loss function is an advanced feature retrieved from the $block5$ layer of the pre-trained LW-Unet.

The perceptual loss function is primarily calculated by comparing the features taken from the image to a LW-Unet network that has already been trained. The following is what we propose:

$$L_p = \frac{1}{H \times W} \sum_{i=1}^{H} \sum_{i=1}^{W} \left[\varphi(\hat{I})_{i,j} - \varphi(I^*)_{i,j}\right]^2 \tag{6}$$

where φ represents the feature map of the pre-trained LW-Unet network. H and W are the height and width of the feature map. The total loss function is expressed as:

$$L = \lambda_1 L_1 + \lambda_2 L_p \tag{7}$$

where $\lambda 1$ and $\lambda 2$ represent the weight of the absolute error loss function and the perceptual loss function in the total loss function, respectively.

4. EXPERIMENTAL RESULTS AND ANALYSIS

4.1 Data set:

The Alzheimer's Disease Neuroimaging Initiative (ADNI) dataset, which is freely accessible online at http://adni.loni.usc.edu, is the data source for this work. With the help of biomarkers, the ADNI hopes to develop more sensitive and precise methods for detecting Alzheimer's disease in its early stages. We employed a total of 694 structural MRI scans for this study, of which 198 were initially categorized as AD, 230 as NC, 166 as pMCI, and 101 as MCI at baseline. The 166 pMCI participants were initially identified as having MCI at baseline, but after a 36-month follow-up, it was discovered that they had converted to AD. The subjects' MMSE scores ranged from 20 to 26 (AD), 24 to 30 (MCI), and 24 to 30 (MCI) for each group, and their ages ranged from 55 to 90.The NACC data set https://www.alz.washington.edu, and the ARWIBO one from https://www.gaaindata.org, which is publicly available on the web. In this work, we used a total of 694 structural MRI scans that were initially classified into AD (n = 122), HCI (n = 130), EMCI (n = 69), and LMCI (n = 54).

4.2. Performance of proposed LW-Unet Model

We have trained the LW-Unet based on Nvidia V100 32GB GPU for 400 epochs with the batch size set to 10. We have conducted 5-fold cross-validation on the dataset of MRI with 80% for training and 20% for testing. Evaluation criteria Various criteria are used to evaluate the performance of the proposed method in determining the AD area. These include dice similarity coefficient (DSC), intersection-Over-Union (IOU) sensitivity, and positive predictive value (PPV) as measured by Eqn(8)

$$\text{IOU} = \frac{\text{TP}}{\text{TP} + \text{FN} + \text{FP}},$$

$$\text{DSC} = \frac{2\text{TP}}{2\text{TP} + \text{FP} + \text{FN}},$$

$$\text{Sensitivity} = \frac{\text{TP}}{\text{TP} + \text{FN}},$$

$$\text{PPV} = \frac{\text{TP}}{\text{TP} + \text{FP}}, \tag{8}$$

where 'TP' is the number of pixels in the true AD area, 'FP' is the number of pixels in the false AD area, 'TN' is the number of pixels in the true non-AD area, and 'FN' is the number of pixels in the false non-AD area.

This study selected different convolutional neural network-based models for training and testing in three different datasets. The convolutional neural network models are AlexNet (Krizhevsky et al, 2018), UNet (Ronneberger et al., 2015), UNet++ (Tulsani et al., 2021), and DeeplabV3+ (Yang et al., 2020)[28-30]. The experimental results of the proposed LW-UNet using the ADNI dataset is given in Table 1 and the NACC dataset is given in Table 2.

Table 1: Detailed Results of the proposed LW-Unet model with different Categories on ADNI Data set

Proposed Models	Accuracy (%)	AUC(%)	Sensitivity (%)	Specificity(%)	F1-Score(%)
AD	98.77	98.96	98.40	98.67	98.12
NCI	97.63	96.56	98.58	97.11	97.33
sMCI	98.54	98.12	97.76	97.43	97.15
pMCI	98.91	97.91	97.36	98.15	98.93

Experimental results of different DCNN models with the ADNI dataset are given in Table 3. As shown in Table 3, the proposed model, which is good at processing medical images, has achieved good classification accuracy, compared with the other models.

Table 2: Detailed Results of the proposed LW-Unet model with different Categories on the NACC and ARWIBO Data set

Propose dModels	Accuracy (%)	AUC(%)	Sensitivity (%)	Specificity(%)	F1-Score(%)
AD	98.45	98.48	97.91	98	98.91
NCI	95.83	94.74	92.56	99	99.21
sMCI	96.43	95.45	92.75	97.12	97.15
pMCI	95	94.87	91.89	92.75	97.93

TABLE 3 Comparisons of AD classification results in different DCNN methods

Models	Sensitivity	Specificity	F1	ACC	AUC
ADNI Data set					
UNet++	0.8628	0.8112	0.7526	0.8157	0.9167
DeeplabV3+	0.6269	0.9821	0.6909	0.9511	0.9534
UNet	0.6851	0.9800	0.7232	0.9543	0.9584
AlexNet	0.6972	0.9889	0.7691	0.9635	0.9769
LW-Unet	0.9879	0.9896	0.9840	0.9840	0.9871
NACC and ARWIBO Data set					
UNet++	0.8823	0.8643	0.8123	0.8412	0.9512
DeeplabV3+	0.7122	0.9712	0.7342	0.9612	0.9712
UNet	0.7841	0.9721	0.8232	0.9612	0.9612
AlexNet	0.7911	0.9767	0.8691	0.9712	0.9811
LW-Unet	0.9812	0.9912	0.9851	0.9891	0.9812

4.3 Comparison with Other State-of-the-Art Methods

In this section, a comparison is shown between the suggested approach and other methods that already exist for detecting AD. In light of the fact that various approaches have been tested on MR images, various handmade feature-based methods and deep learning-based methods for the identification of AD in MRI images have been selected. In Table 4, we compare the findings of the ADNI dataset with those obtained by several current methodologies. In the approaches that are now in use, the detection of an AD candidate comes first, followed by the collection of characteristics that are used to determine if the candidate is normal or abnormal. As can be shown in Table 4, the suggested technique achieves superior detection results when compared to other methods already in use for detecting nodules using MR imaging.

Table 4 : AD Classification results of the proposed method and state-of-the-art methods

Model	Accuracy	Recall	Precision	F1-score	AUC
Liu et al. (2018)	92.65	92.88	92.10	91.34	89.34
Liu et al. (2020)	93.54	92.73	93.35	93.01	90.50
Xia et al. (2020)	97.22	96.63	97.01	96.81	95.64
Kruthika et al. (2019)	95.58	95.52	94.78	95.12	93.15
Zhang et al. (2019)	95.75	94.91	95.08	94.96	93.36
Proposed (LW-Net)	**98.79**	**98.96**	98.40	99	99.8

The AD classification visualization results of the proposed LW-Unet model are given in Figure 6. . Furthermore, as shown in Fig. 6, the age difference allowance for constructing an edge can be varied to adjust the degree of connection restriction between nodes. With the large age difference allowance, the connection restriction should be loose, which results in more edges for each node, and vice versa.

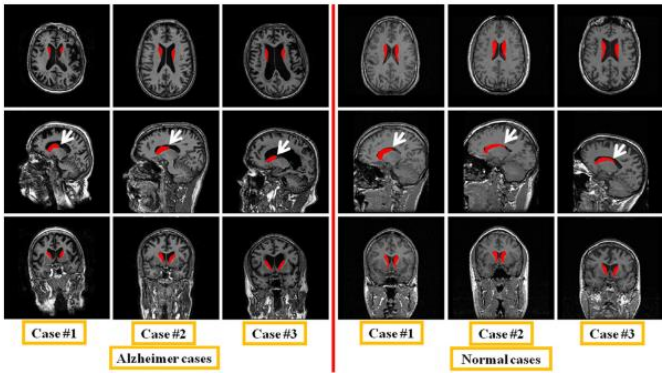

Fig. 6. Visual comparison of AD classification produced by LW-Unet frameworks.

5 . CONCLUSION

In the current study, a new pipeline methodology was offered for the automatic classification of AD from MRI images. The process starts with a pre-processing stage including noise reduction and contrast enhancement and then it is fed to the main process. We propose an LW-Unet work for AD classification using MRI images, which has proved effective owing to the performance improved by deep learning algorithms with types of different types of classes for AD diagnosis. The experimental results also show that our proposed Lightweight UNet-based node classifier with graphs constructed from the image and phenotypic data has the best performance. In order to verify the effectiveness of the improvements made to the U-Net network, three comparative experiments were designed: the comparison test of the LW-Unet network model and other classic classification network models in terms of classification performance conducted ablation experiments on different improved modules and verified the performance of the loss function in terms of classification. The number of network layers and parameters is effectively decreased by connecting the internal convolutional layers in parallel. To boost prediction abilities, Dense Block is specifically used to extract rich low-level characteristics. The suggested decoder reduces boundary loss and degree of overfitting in image classification by fusing multi-scale semantic information to restore image details. Extensive testing on the ADNI dataset shows that our suggested strategy performs better than the state of the art.

REFERENCES

[1] Cheng, J., Liu, Z., Guan, H., Wu, Z., Zhu, H., Jiang, J., Wen, W., Tao, D., Liu, T., 2021. Brain age estimation from mri using cascade networks with ranking loss. IEEE Transactions on Medical Imaging 40, 3400–3412.

[2] Gorji T. H., Naima K. A deep learning approach for diagnosis of mild cognitive impairment based on MRI images. Brain Sciences. 2019;9(9):p. 217.

[3] Guévremont, D.; Tsui, H.; Knight, R.; Fowler, C.J.; Masters, C.L.; Martins, R.N.; Abraham, W.C.; Tate, W.P.; Cutfield, N.; Williams, J.M. Plasma microRNA vary in association with the progression of Alzheimer's disease. Alzheimer's Dement. 2022, 14, e12251.

[4] Gupta Y., Lee K. H., Choi K. Y., Lee J. J., Kim B. C., Kwon G.-R. Alzheimer's disease diagnosis based on cortical and subcortical features. Journal of Healthcare Engineering. 2019;2019:13.

[5] Ho, N.H., Yang, H.J., Kim, J., Dao, D.P., Park, H.R., Pant, S., 2022. Predicting progression of alzheimer's disease using forward-to-backward bidirectional network with integrative imputation. Neural Networks 150,422–439.

[6] Janousova, E.; Vounou, M.; Wolz, R.; Gray, K.R.; Rueckert, D.; Montana, G. Biomarker discovery for sparse classification of brain images in Alzheimer's disease. Ann. BMVA 2012, 2, 1–11.

[7] Khojaste-Sarakhsi, M., Haghighi, S.S., Ghomi, S.F., Marchiori, E., 2022. Deep learning for alzheimer's disease diagnosis: A survey. Artificial Intelligence in Medicine , 102332.

[8] Klöppel, S.; Stonnington, C.M.; Chu, C.; Draganski, B.; Scahill, R.I.; Rohrer, J.D.; Fox, N.C.; Jack, C.R., Jr.; Ashburner, J.; Frackowiak, R.S. Automatic classification of MR scans in Alzheimer's disease. Brain 2008, 131, 681–689.

[9] A.J. Prabhu and A. Jayachandran, Mixture model segmentation system for parasagittal meningioma brain tumor classification based on hybrid feature vector, Journal of Medical System 42(12) (2018)..

[10] Li, W., Lin, X., Chen, X., 2020. Detecting alzheimer's disease based on 4d fmri: An exploration under deep learning framework. Neurocomputing 388, 280–287.

[11] Liu, C., Huang, F., Qiu, A., Initiative, A.D.N., et al., 2023. Monte carlo ensemble neural network for the diagnosis of alzheimer's disease. Neural Networks 159, 14–24.

[12] Liu, S.; Song, Y.; Cai, W.; Pujol, S.; Kikinis, R.; Wang, X.; Feng, D. Multifold Bayesian kernelization in Alzheimer's diagnosis. In Proceedings of the International Conference on Medical Image Computing and Computer-Assisted Intervention, Nagoya, Japan, 22–26 September 2013; Springer: Berlin/Heidelberg, Germany, 2013.

[13] Michaud, T.L., Su, D., Siahpush, M., Murman, D.L., 2017. The risk of incident mild cognitive impairment and progression to dementia considering mild cognitive impairment subtypes. Dementia and geriatric cognitive disorders extra 7, 15–29.

[14] Nozadi S. H., Kadoury S. Classification of Alzheimer's and MCI patients from semantically parcelled PET images: a comparison between AV45 and FDG-PET. International Journal of Biomedical Imaging. 2018;2018:13.

[15] Pan, X., Phan, T.L., Adel, M., Fossati, C., Gaidon, T., Wojak, J., Guedj, E., 2020. Multi-view separable pyramid network for ad prediction at mci stage by 18 f-fdg brain pet imaging. IEEE Transactions on Medical Imaging 40, 81–92.

[16] Park, J.H., Cho, H.E., Kim, J.H., Wall, M.M., Stern, Y., Lim, H., Yoo, S., Kim, H.S., Cha, J., 2020. Machine learning prediction of incidence of alzheimer's disease using large-scale administrative health data. NPJ digital medicine 3, 46.

[17] Parmar, H., Nutter, B., Long, R., Antani, S., Mitra, S., 2020a. Spatiotemporal feature extraction and classification of alzheimer's disease using deep learning 3d-cnn for fmri data. Journal of Medical Imaging 7, 056001.

[18] Parmar, H.S., Nutter, B., Long, R., Antani, S., Mitra, S., 2020b. Deep learning of volumetric 3d cnn for fmri in alzheimer's disease classification, in: Medical Imaging 2020: Biomedical Applications in Molecular, Structural, and Functional Imaging, SPIE. pp. 66–71.

[19] A. Jayachandran and R. Dhanasekaran, Automatic detection of brain tumor in magnetic resonance images using multi texton histogram and support vector machine, International Journal of Imaging Systems and Technology 23(2) (2013), 97–103..

[20] Qiu, A.; Fennema-Notestine, C.; Dale, A.M.; Miller, M.I. Regional shape abnormalities in mild cognitive impairment and Alzheimer's disease. Neuroimage 2009, 45, 656–661.

[21] Risacher, S.; Saykin, A.; Wes, J.; Shen, L.; Firpi, H.; McDonald, B. Baseline MRI Predictors of Conversion from MCI to Probable AD in the ADNI Cohort. Curr. Alzheimer Res. 2009, 6, 347–361.

[22] Ronneberger O, P. Fischer, T. Brox, U-net: Convolutional networks for biomedical image segmentation, Proc. Int. Conf. Med. Image Comput. Comput.-Assisted Intervent., (2015) 234-241.

[23] Tulsani A, P. Kumar, S. Pathan, Automated segmentation of optic disc and optic cup for glaucoma assessment using improved unet++ architecture, Biocybern Biomed Eng 41 (18),2021.

[24] Wang, C., Li, Y., Tsuboshita, Y., Sakurai, T., Goto, T., Yamaguchi, H.,Yamashita, Y., Sekiguchi, A., Tachimori, H., Initiative, A.D.N., 2022. A high-generalizability machine learning framework for predicting the progression of alzheimer's disease using limited data. NPJ digital medicine 5, 43.

[25] Xia, Z., Yue, G., Xu, Y., Feng, C., Yang, M., Wang, T., Lei, B., 2020. A novel end-to-end hybrid network for alzheimer's disease detection using 3d cnn and 3d clstm, in: 2020 IEEE 17th International Symposium on Biomedical Imaging (ISBI), IEEE. pp. 1–4.

[26] Yang Z, X. Peng, and Z. Yin, "Deeplab v3 plus-net for image semantic segmentation with channel compression," in Proceedings of IEEE 20th International Conference on Communication Technology (ICCT). IEEE, 2020, pp. 1320–1324.

[27] Zhang, D.; Wang, Y.; Zhou, L.; Yuan, H.; Shen, D. Multimodal classification of Alzheimer's disease and mild cognitive impairment. Neuroimage 2011, 55, 856–867.

[28] Zhang, F., Li, Z., Zhang, B., Du, H., Wang, B., Zhang, X., 2019. Multimodal deep learning model for auxiliary diagnosis of alzheimer's disease. Neurocomputing 361, 185–195

[29] Zhang, Y.; Dong, Z.; Phillips, P.; Wang, S.; Ji, G.; Yang, J.; Yuan, T.-F. Detection of subjects and brain regions related to Alzheimer's disease using 3D MRI scans based on eigenbrain and machine learning. Front. Comput. Neurosci. 2015, 9, 66.

[30] Zhu,W., Sun, L., Huang, J., Han, L., Zhang, D., 2021. Dual attention multiinstance deep learning for alzheimer's disease diagnosis with structural mri. IEEE Transactions on Medical Imaging 40, 2354–2366.

[31] A. Jayachandran and R. Dhanasekaran, Brain tumor detection using fuzzy support vector machine classification based on a texton co-occurrence matrix, Journal of imaging Science and Technology 57(1) (2013), 10507-1–10507-7(7).